# Numerical linked cluster expansions for the transverse field Ising model

Bachelor's thesis in physics

Presented by
**Markus Pirke**
05.08.2022

Institute für Theoretische Physik I
Friedrich-Alexander Universität Erlangen-Nürnberg


Supervisor: Prof. Dr Kai P. Schmidt

# Abstract

In this work we introduce the method of numerical linked cluster expansions. This is an approach to calculate extensive properties, in the thermodynamic limit, where one does an exact diagonalization on many small clusters. Here we also briefly introduce the transverse field Ising model and then set up the basic building blocks for the expansion, like graph theory, linked cluster expansions and exact diagonalization. To illustrate this procedure and also show results of calculations, we do a numerical linked cluster expansion to calculate properties for the transverse field Ising model on a chain and the triangular lattice. We compare these calculations to exact results for the chain and to series expansions for the triangular lattice.

# Contents

**1 Introduction** **4**

**2 Transerverse field Ising model** **6**

**3 Methods** **8**
3.1 Basic Graph theory . . . . . 8
3.2 Linked Cluster Expansion . . . . . 9
3.3 Graph generation . . . . . 10
3.4 Exact Diagonalization . . . . . 10
3.4.1 Building the Hamiltonian . . . . . 11
3.4.2 Algorithm for Diagonalization . . . . . 12

**4 Results** **13**
4.1 Ground state energy for different geometries . . . . . 13
4.1.1 TFIM on a chain . . . . . 13
4.1.2 TFIM on a triangular lattice . . . . . 14
4.1.3 Numerical Issues . . . . . 18
4.2 Second derivative ground state energy . . . . . 20

**5 Conclusions and Outlook** **24**

**A Julia Programming Language** **25**

**B Algebraic fit** **26**

# Chapter 1

# Introduction

> "What we observe is not nature itself, but nature exposed to our method of questioning"
>
> Werner Heisenberg

The goal of theoretical physics is to predict the future. By that we mean that we can ask questions to nature, in terms of experiments, and our theory should tell us what is going to happen. In principal, there should be one theory for all such questions one could ask. This theory is yet to be found. At the moment we have two well tested theories, which describe nearly all phenomena in nature. One theory describes gravity and is called the general theory of relativity (GR) introduced by Einstein in 1915 [1]. All other forces in nature are explained within the standard model of particle physics, which was developed throughout the whole twentieth century by Feynman, Gell-Mann, Weinberg among many others. However, in the high energy regime, where both gravity and quantum mechanics become important, these theories clash. GR is a purely classical theory whereas the Standard model is a quantum field theory. It turns out that those two are not compatible. Still, in our day to day experience we usually do not encounter things happening at these high energy scales. Otherwise we would not be here.

In the low energy regime the theory of everything is basically known since the late 1920s when Schrödinger, Heisenberg, Dirac and others established the theory of quantum mechanics. We can in principal write down the equation governing all phenomena in low energy physics. Namely Schrödingers equation. It is a linear partial differential equation and the problem is that even for relatively simple systems, like a molecule with a only few atoms, Schrödingers equation is really hard to solve.

The problem gets worse, if we want to understand emergent macroscopic properties. Macroscopic properties usually cannot be explained from just a few atoms. An example of an emergent property is the wetness of water. We are not able to explain this property by just looking microscopically at just a few atoms at a time. In this microscopic regime it makes no sense to talk about wetness. To explain the wetness of water directly from the fundamental law, the Schrödinger equation, we would need to solve this equation for $10^{23}$ interacting atoms, which is, for all practical cases, not possible. That emergent properties are hard to predict from a microscopic theory is not only true for our example of water, but is a quite general observation. This phenomenon was discussed in a paper in 1972 from P. W. Anderson, where he coined the term "more is different". There he writes: "The ability to reduce everything to simple fundamental laws does not imply the ability to start from those laws and reconstruct the universe"[2]

That is why we look at approximative models to describe certain phenomena in condensed matter physics. One of such models is the Ising model. It is probably the most studied one in all of statistical physics. Other models used in condensed matter physics are for example the Heisenberg model or the Hubbard model. Even for those approximated models in general no analytic solution can be found. Therefore, approximative methods to solve models describing quantum many body problems are needed. Many of those have been developed since the quantum theory has been established in 1925. Examples are Rayleigh Schrödinger pertubation theory, general series expansion techniques [3] and quantum Monte Carlo simulations (QMC) [4]. Another such method is called a Numerical Linked Cluster Expansion (NLCE) [5][6]. In general Linked Cluster Expansion (LCE) can be used to calculate extensive properties of lattices models. A quantity is extensive if it is proportional to the system sizes. Examples are energy, entropy and volume. A NLCE is therefore a special case of a LCE where on every cluster one calculates

certain properties numerically via an exact diagonalization (ED).

In this thesis we explain how one can use an NLCE to calculate properties of the transverse field Ising model (TFIM) for different lattice geometries, starting with a chain and then going to the triangular lattice. In the next chapter we first introduce the transverse field ising model. Then in the third chapter we explain the steps and methods needed to set up an NLCE. The fourth chapter is dedicated to the results for different lattices. In the last chapter we draw conclusions and give an outlook for future ideas.

# Chapter 2

# Transerverse field Ising model

Before we introduce the TFIM, we briefly mention some historical discoveries that predated the introduction of the TFIM. It probably all started with the discovery of a certain type of rock, magnetite ($Fe_3O_4$). A type of rock with peculiar properties. It attracts iron or steel and sometimes different magnetites repell each other. These phenomena were certainly known by the Greeks since the year 800 B.C., where the name loadstone first appeared in Greek writings [7][8]. However, the first to do real experiments, by the standards of todays defintion, was William Gilbert. He published his finding in a famous book called DeMagnete in 1600, where he has already written that even the earth itself acts as a magnet [9]. In the following years many experiments on magnetism were made by people like Ampere, Oersted and probably most famously Faraday. In 1873 James Clerk Maxwell published his work, where he unified three phenomena of nature. Electric and magnetic phenomena and light were then combined in one theory of electromagnetism [10]. However, certain properties of magnets could still not be explained. For example: Why does a ferromagnet lose its properties if one heats it up above a certain temperature? This behavior is known as a phase transition, where macroscopic properties of a system change as one varies some external parameter. For a ferromagnet the magnetization changes as the temperature varied. To explain this phase transition, a microscopic theory of magnetism was needed. One of the first attempts of such a theory was made by Wihelm Lenz in 1925, where he introduced the Ising model as a problem for his PhD student Ernst Ising [11]. The Ising model is defined on a lattice and the energy of the system is defined as:

$$E = -J \sum_{<i,j>} S_i S_j + h \sum_i S_i \tag{2.1}$$

$S$ represents a spin state which can either be $+1$ or $-1$. The sum over $< i, j >$ denotes summing over the nearest neighbours. $J$ and $h$ are parameters. $J$ determines the strength of the interaction between neighbouring spins, while $h$ determines the strength of an external field. For $J > 0$ we speak of an ferromagnet, for $J < 0$ of an antiferromagnet. In his PhD thesis Ising found out that for a one dimensional lattice the model does not exhibit a phase transition. However, a few years later, Onsager showed that for the two dimensional Ising model there is a phase transition at a finite temperature $T_C$, which is in close resemblance to a real ferromagnet [12]. We know phase transitions from our day to day experience. Water changes to steam if one heats it up over a certain temperature. So there is a phase transition from the liquid state to a gasous state at a temperatue $T_C$. Classical phase transitions are best described in the language of statistical mechanics. In that language a phase transition is defined as a point where the free energy $F$ is non analytic. One then distinguishes between two kinds of phase transitions. First order and second order phase transitions. In a first order phase transition the first derivative of the free energy is discontinuous. Whereas in a second order phase transition the first derivative is still continuous, but the second derivative is not. This classification was introduced by Ehrenfest in 1933, after the discovery of the phase transition in liquid helium [13]. In this classification the phase transition in water is of first order and the one in the Ising model of second order. Another well known second order phase transition happens if one cools down a metal below a certain temperature. Above the critical temperature $T_c$ the metal is an ordinary conductor. However, below the critical temperature the metal becomes a perfect conductor without any resistance. This discovery has led to a number of applications. Superconductors are used in magnetic resonance imaging (MRI), at the LHC in Cern and in Superconducting Qubits. From those examples we see that unterstanding phase transitions

is not only of academic interest, but also finds applications in industry.

Now, all of the phase transitions mentioned happen due to changes in temperature. There are also phase transitions happening at zero temperature. We call those quantum phase transitions (QPTs). For QPTs, compared to classical phase transitions the important quantity is not the free energy, but the ground state energy of the system, because the free energy is not a well defined quantity at zero temperature. The classification of first and second order phase transition remains the same, just the free energy is replaced by the groundstate energy. The TFIM, at temperatue $T = 0$ and spin-half degrees of freedom S=1/2, is the prototypical model for a QTPs. Here we look at a system which changes its properties as an external applied field is varied. As for the classical Ising model the TFIM is also defined on a lattice. The Hamiltonian of the TFIM is defined as:

$$H = -J \sum_{<i,j>} \sigma_i^z \sigma_j^z - h \sum_i \sigma_i^x \tag{2.2}$$

The sum over $< i, j >$ again denotes summing over nearest neighbours. The $\sigma_i^\alpha$ with $\alpha \in \{x, z\}$ are the Pauli matrices. $J$ and $h$ are the parameters of the model. $J$ is an exchange interaction between neighbouring spins and $h$ is the strength of the external magnetic field. Again we speak of an ferromagnet if $J > 0$ and of an antiferromagnet if $J < 0$. Here we want to use units in which $h = 1$. Therefore the Hamiltonian is written as:

$$H = -J \sum_{<i,j>} \sigma_i^z \sigma_j^z - \sum_i \sigma_i^x \tag{2.3}$$

This model was first introduced by de Gennes in 1963 to describe hydrogenbonded ferroelectrics, such as $KH_2PO_4$ [14]. In these systems the proton sits in a minimum of a double well potential. The transverse-field term allows for tunneling between the two wells, and the exchange term represents the correlation energy of possible proton arrangements [15]. For the coming calculations it will be easier if we rewrite the Hamiltonian as

$$H = \sum_i (1 - \sigma_i^z) - J \sum_{<i,j>} \sigma_i^x \sigma_j^x \tag{2.4}$$

where we have changed the indices $x$ and $z$ and also added an extra constant term. The constant term does not change the physics as we are only interested in energy differences. In this representation we see that the Hamiltonian can be written as $H = H_0 + JV$, where $H_0 = \sum_i (1 - \sigma_i^z)$. This term is already diagonal in the $z$ basis where the Pauli matrix $\sigma^z = \mathrm{diag}(1, -1)$. From this we immediately see that if there are no interactions between the neighbouring spins ($J = 0$) the Hamiltonian is diagonal. The ground state of the system is the state in which all spins are aligned in direction of the applied magnetic field and the ground state energy $E_0 = 0$. The second term is $V = \sum_{<i,j>} \sigma_i^x \sigma_j^x$ which does not commute with $H_0$. This non commutative term is the cause for quantum fluctuations, which induce the quantum phase transition. The model is exactly solvable in one dimension, i.e. on a chain. For higher dimensions there is in general no exact solution and therefore approximations have to be applied. As already mentioned we want to estimate ground state properties of the TFIM with the help of a NLCE, which we introduce in the next chapter. As a last remark, there is a interesting connection between the TFIM and the classical Ising model. The TFIM in d dimensions can be mapped to the classical Ising model in d+1 dimensions. For example the TFIM in zero dimensions is just a two level system. This two level system can be mapped to the classical Ising chain [16].

# Chapter 3

# Methods

As already mentioned in the introduction we want to calculate properties of the TFIM by means of a numerical linked cluster expansion (NLCE). The main idea is that instead of doing calculations on the whole lattice, we calculate properties on small sublattices and add them up to get a good approximation for properties in the thermodynamic limit. In this chapter we introduce all tools we need for the NLCE. We start with basics of graph theory and linked cluster expansions. After these two building blocks we discuss the method of Exact Diagonalization (ED).

## 3.1 Basic Graph theory

A lattice is a set of points, which are ordered in a periodic fashion. Now if we also think about our model which lives on a lattice, we have on each point on the lattice a spin which can be either up or down. Each spin interacts with its neighbouring spins. The lattice together with these interactions can be represented as a graph. The following graph theoretic definitions are based on a book by Deo Narsingh [17]. Mathematically a graph $G = (V, E)$ is defined as a set of objects $V = \{v_1, v_2, ...\}$ called vertices and a set $E = \{e_1, e_2, ...\}$ containing edges $e_i$. Each edge $e_i$ consists of a tuple $(v_i, v_j)$ of vertices. Going back into the picture of spins on a lattice and interactions between them, we can now think of a spin on a lattice as a vertex of a graph and the interactions between spins as edges connecting those vertices. A graph with N vertices is said to be of order N ($O(N)$) and a vertex, which is connected to $k$ edges, is of degree $k$. We differentiate between two kinds of graphs. Connected or linked graphs and disconnected graphs. A graph is connected or linked if we can travel from any vertex to any other vertex along the edges. Otherwise the graph is disconnected. And as a last definition we say $G'$ is a subgraph of $G$ if all vertices and edges of $G'$ are included in $G$. To get a better understanding of these definitions two

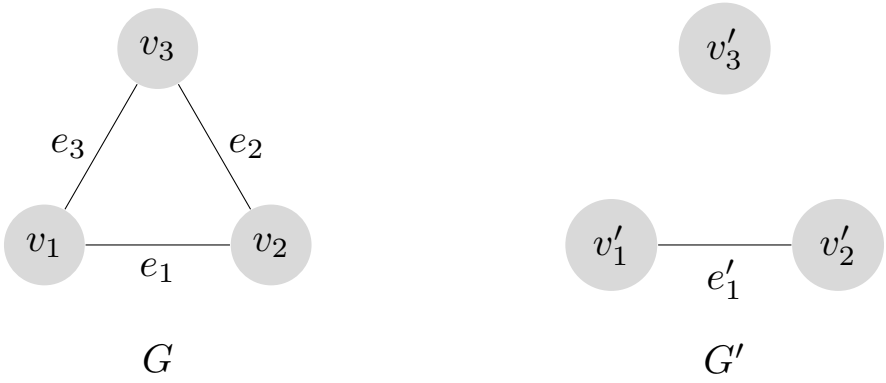


Figure 3.1: Basic graphs. The left graph G is a connected graph of order 3 and every vertex is of degree three. Meanwhile the right graph $G'$ is disconnected and of order 2. The vertices $v'_1, v'_2$ are of degree 1, while $v'_3$ has degree zero. $G'$ is also a subgraph of $G$. Both graphs are also subgraphs of the triangular lattice.

graphs are shown in figure 3.1. $G$ is a connected graph, while $G'$ is disconnected. The order of graph

$G$ is three and has only vertices of degree two. $G'$ is also of order three, but the vertices $v_1', v_2'$ are of degree 1 and the third vertex $v_3$ has degree zero. $G'$ is also a subgraph of $G$. In addition both of these graphs are subgraphs of the triangular lattice. Having established the basic language of graph theory, we can now introduce linked cluster expansions.

## 3.2 Linked Cluster Expansion

Cluster expansions were originally introduced by Mayer in the late 1930s [18]. He was a physical chemist and an expert in statistical physics. He was particularly interested in statistical mechanics of imperfect gases. There he and colaborators introduced methods based on graphs for computing coefficients of virial series for various thermodynamic properties [19]. Another form of cluster expansion was introduced by Richard Feynman a few yeas later, the Feynman diagrams [20]. They were first used as a bookkeeping tool in quantum electro dynamics (QED). Nowadays Feynman diagrams are one of the most used tools for calculations in general quantum field theories. Each diagram represents a physical process. Adding up many of these schemactic processes gives you a good approximations of a real physical process in nature.

The idea in a linked cluster expansion for lattice models is similar. We want to approximate properties in the thermodynamic limit, i. e. on an infinite lattice, as a sum over subgraphs or clusters. The hope is then that one includes all physical processes which are most likely to happen on these smaller clusters. This method was introduced by Marland in 1981 [21] and has since been used extensivly by Irving, Hamer and Singh in the following years [22] and also more recently by Schmidt and others [23][24]. Now we introduce the method in detail and we follow the book "Series expansion methods for strongly interacting lattice models" by Oitmaa, Hamer and Zheng [3]. We consider a Hamiltonian of the form:

$$H = H_0 + \lambda V \tag{3.1}$$

For $H_0$ we know the eigenenergies. Then we can calculate the ground state energy per site, in the thermodynamic limit $N \to \infty$, as a sum over small clusters:

$$\frac{E_0}{N} = \sum_{\{G\}} C(G)\epsilon(G) \tag{3.2}$$

Here $E_0$ is the ground state energy, $\{G\}$ denotes summing over all subgraphs of the lattice and $\epsilon(G)$ is the reduced energy of the cluster $G$. The factor in front of the reduced energy $C(G)$ is the embedding factor for the subgraphs. It counts how often a subgraph can be embedded onto the whole lattice. We now use the same expansion 3.2 to calculate the reduced energies $\epsilon(G)$. The reduced energy of the smallest graph is just the ground state energy of the graph. For each subgraph $G$ we can also write down a linked cluster expansion:

$$E(g) = \sum_{G' \in G} C\left(\frac{G'}{G}\right)\epsilon(G') \tag{3.3}$$

$E(g)$ denotes the ground state energy of the subgraph $G$ and we are summing over all subgraphs $G'$ of $G$. $C\left(\frac{G'}{G}\right)$ counts how many times the graph $G'$ can be embedded in the bigger graph $G$. Now we can use 3.3 recursivly to calcuate the reduced energies up to the smallest subgraph. Up to now we have only specified that we need to sum over all subgraphs of a lattice. It turns out for extensive properties we can reduce the number of subgraphs in the sum drastically. The ground state energy is an extensive quantity. Thus the ground state energy of a graph $G$, which can be decomposed as the sum two graphs $G_1$ and $G_2$ is the same as the ground state energy of both graphs individually and then taking the sum of the energies. So we have

$$E(G) = E(G_1 + G_2) = E(G_1) + E(G_2) \tag{3.4}$$

This property is known as the cluster addition property. With 3.4 we can now proof that the reduced energy for disconnected clusters vanishes.

$$\begin{aligned} \epsilon(G) = \epsilon(G_1 + G_2) &= E(G_1 + G_2) \quad - \sum_{G' \in G, G' \neq G} C(G'/G)\epsilon(G') \\ &= E(G_1 + G_2) - E(G_1) - E(G_2) = 0 \end{aligned} \tag{3.5}$$

## 3.3 Graph generation

For the LCE we need to generate all subgraphs of a certain lattice which are not related by point symmetries and are not topological equivalent. Point symmetries are for example reflections or rotations. By topological distinct we mean that two subgraphs cannot be deformed into each other without breaking or making new bonds. In order to illustrate these two concepts we look at a few examples.

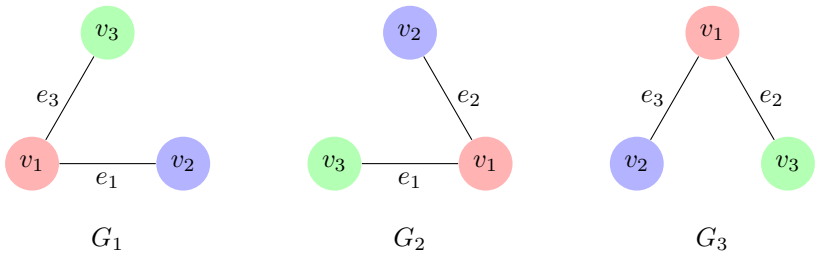


Figure 3.2: Symmetric graphs: All three graphs are subgraphs of the triangular lattice and are related by some kind of rotation. If we rotate $G_1$ by 120 degrees counterclockwise we get $G_2$. Rotating it by 240 degrees counterclockwise we get $G_3$. The nodes are coloured to see the rotations more easily. Therefore the three graphs are symmetric and only one graph should be included in the LCE.

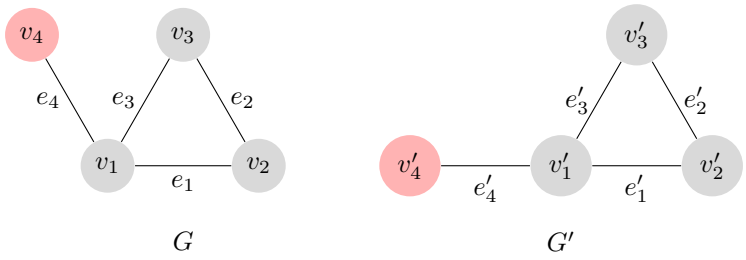


Figure 3.3: Topologically equivalent graphs: $G$ as well as $G'$ are subgraphs of the triangular lattice. The two graphs $G$ and $G'$ can be deformed into each other, because the only difference between those is the position of the red nodes. But these nodes have the same distance to the bottom left node in the triangle where they are both connected to. Therefore they are topologically equivalent to each other and should only be counted once in the LCE.

The three graphs in figure 3.2 can be transformed into each other by a point symmetry. Graphs $G_1$ and $G_2$ are related by a 120 degree rotation. $G_1$ and $G_3$ by a rotation of 240 degrees. Figure 3.3 shows two topologically equivalent graphs, the only difference is the position of the red node. We can deform these into each other, because the two positions of the red nodes have the same distance to the bottom left node of the triangle. Only taking into account topological distinct graphs, reduces the number of subgraphs drastically, but also complicates an algorithm for finding all subgraphs. A general explanation for generating all topologically equivalent graphs is given in [25]. However, there is in general no simple argument to decide whether two graphs are topological equivalent or not. Here the graphs are generated by Matthias Mühlhauser. The algorithm generates a bondfile and a subgraph file for each graph. The bondfile includes the set of vertices and edges, while the subgraph file lists all subgraphs of the graph. In addition the embedding factors for the graph and all its subgraphs are included. These factors take into account the many possible ways of embedding the graph on the lattice and also the variety of possibilities all subgraphs can be embedded on the graph itself.

## 3.4 Exact Diagonalization

Given the expression for the ground state energy in the thermodynamic limit in the form of a LCE, the task is now to calculate the ground state energy of all clusters. The usual approach is to make a series expansion around the high field limit. Here we take a different approach, namly doing an exact diagonalization (ED) on every cluster, hence the name numerical linked cluster expansion (NLCE). From

the discussion of the TFIM, we know that the Hilbert space is growing exponentially. The dimension of the Hamiltonian for a cluster with $N$ sites is $2^N$ times $2^N$. Even storing the whole matrix for relatively small $N$ becomes a challenge. Take $N = 15$ as an example, the hamiltonian is now a $2^{15}$ times $2^{15}$ matrix. Naively storing every entry of the matrix as a Float64 one needs $2^{15}$ times $2^{15}$ times 8 Byte of memory, which is already the maximum a computer with 8GB of RAM could handle.

### 3.4.1 Building the Hamiltonian

The previous section showed that storing the whole Hamiltonian is not an option. However, for the TFIM one can use the fact that most of the matrix entries are zero. Indeed the number of non-zero entries divived by the number of all entries tends to zero exponentially as shown in figure 3.4. Therefore

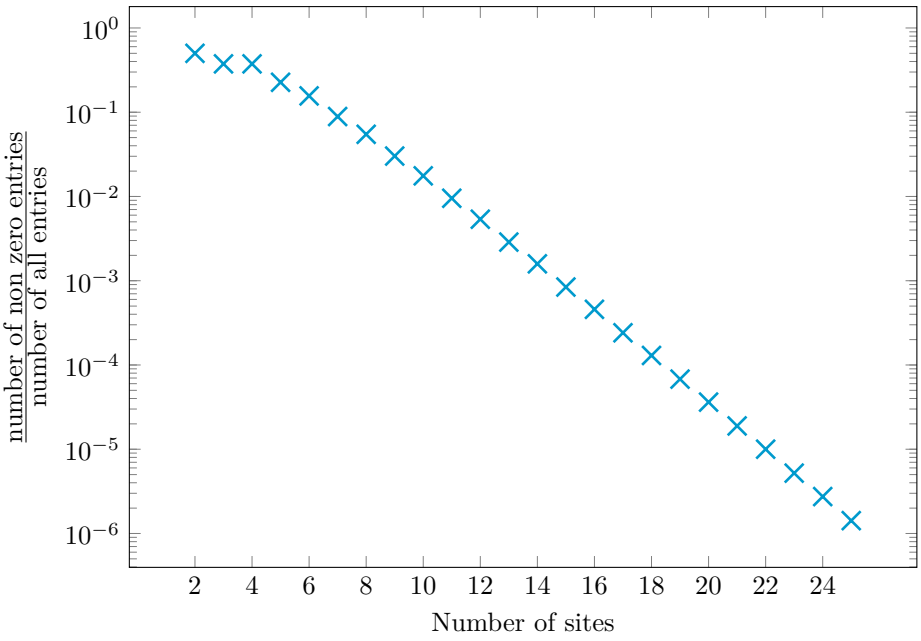


Figure 3.4: Non zero entries in hamiltonian of the TFIM. Here we see that the entries of the Hamiltonian of the TFIM are mostly zero as we increase the number of sites.

the Hamiltonian should be stored as a sparse array. Sparse arrays are efficient data types for storing vectors or matrices which have a specific structure. As a simple example take a vector of length 100 where all entries are one. Storing this vector as a regular array of Float64 it takes 100 times 8 Byte of memory. Alternatively, the vector can be stored with only two numbers. One determines the length of the vector and the other specifices the entries, which can be done as all entries are the same. This can also be applied to more complicated matrices, as in our case, the Hamiltonian for the TFIM. The building blocks of the Hamiltonian of the TFIM are the Pauli matrices, $\sigma^x$ and $\sigma^z$, together with the identity. In the $z$ basis these can be represented as two by two matrices:

$$\sigma^x = \begin{pmatrix} 0 & 1 \\ 1 & 0 \end{pmatrix}, \quad \sigma^z = \begin{pmatrix} 1 & 0 \\ 0 & -1 \end{pmatrix}, \quad \mathbb{1} = \begin{pmatrix} 1 & 0 \\ 0 & 1 \end{pmatrix}$$

To build the whole Hamiltonian in this basis, we store these three matrices as sparse arrays und explicitely calculate all the tensor or Kronecker products. One drawback of this approach is that the whole Hamiltonian needs to be stored as one matrix in memory. A different approach would be to calculate matrix elements $H_{ij} = \langle i | H | j \rangle$ one at a time. That way we can make use of symmetries to block-diagonalize the Hamiltonian. This approach would be needed if one wants to calculate energies for clusters with around 25 sites or more. However, here the limiting factor is not memory. The bigger problem is the number of clusters needed to be calculated for a certain order. The number of clusters is growing exponentially with the number of sites. Therefore, the limiting factor is CPU time rather than memory.

### 3.4.2 Algorithm for Diagonalization

Now that we have implemented the Hamiltonian and saved it in memory, we need to calculate the ground state energy. In other words we need to diagonalize a matrix. So we have the following problem: Given a matrix A we need to find scalars $\lambda$ and vectors $v$ such that

$$Av = \lambda v$$

$\lambda$ is called the eigenvalue corresponding to the eigenvector $v$. In physics and also in engineering many problems one has to solve can be written in terms of an eigenvalue problem. For example a vibrating string, analyzing a big dataset, calculating moments of inertia and in our case solving Schrödingers equation.

$$H\left|n\right\rangle = E_n\left|n\right\rangle$$

where H is the Hamiltonian, $|n\rangle$ the eigenvectors corresponding to the eigenvalue $E_n$. Most of these problems can not be solved by hand anymore. Even for matrices as big as four times four the calculations get very tedious. Therefore we have no chance at all diagonalizing the Hamiltonian of the TFIM analytically for more then three sites. As eigenvalue problems turn up frequently in science, many algorithms have been introduced to solve for eigenvalues numerically. For large and sparse matrices algorithms based on projection methods are the most popular. They are particullary useful if one only wants to calculate eigenvalues at the beginning or the end of the whole spectrum. In other words if one is only interested in the smallest or largest eigenvalues. As we are interested in the ground state energy of the TFIM which is the lowest energy and hence the lowest eigenvalue, these methods will be used here. Here an important class of projection methods are based on the Krylov subspace, which is defined as

$$K_m = span\left\{v, Av, A^2v, ..., A^{m-1}v\right\} \tag{3.6}$$

For numerical stability the vectors spanning the Krylov subspace will usually be orthoganalized by some kind of Gram-Schmidt algorithm [26]. Two famous algorithms for calculating eigenvalues which rely on the Krylov subspace are Arnoldi's method and Lanczos algorithm. In this thesis we use Arnoldis's method and a package called ArnoldiMethod.jl written in the Julia programming language. For a brief introduction to the Julia programming language see Appendix A.

# Chapter 4

# Results

## 4.1 Ground state energy for different geometries

An important quantity of a quantum mechanical system is the ground state energy. It is the lowest possible energy of the system. For quantum many body systems it is in general an exponentially hard problem, meaning there exists no algorithm which calculates the ground state energy in polynomial time on a classical computer. It is even worse. It is also very unlikely that we will find an algorithm to solve the problem efficiently on a quantum computer [27]. With that in mind, this is the first quantity we want to approximate for the TFIM with an NLCE.

### 4.1.1 TFIM on a chain

We start our calculation with the simplest of all lattices, a chain. The lattice is shown in figure 4.1. We start with this lattice for two reasons. First, for the chain it is easy to generate all subgraphs and the corresponding embedding factors $C(G)$. The subgraphs $G$ of the chain, are just chain segments of a certain length. The first few chain segments are shown in figure 4.2. We can even give an explicit formula for the embedding factors. A chain segment of length $n$ can be embedded $C\left(\frac{G_n}{G_m}\right)$ times on a chain segment of length $m$, where this factor is calculated as

$$C\left(\frac{G_n}{G_m}\right) = m - n + 1 \tag{4.1}$$

The second reason for studying the chain first is that this geometry is exactly solveable. In 1970 Pierre Pfeuty published a paper where he transformed the TFIM into a system of noninteracting Fermions. Then, he showed that the ground state energy can be expressed with an elliptic integral of second kind [28].

$$\frac{E_0}{N} = -J\frac{2}{\pi}(1+\lambda)E\left(\frac{\pi}{2},\theta\right) \qquad \text{with} \qquad \theta^2 = \frac{4\lambda}{(1+\lambda)^2},\ \ \lambda = 1/J \tag{4.2}$$

The elliptic integral in 4.2 is nonanalytic for $\theta = 1 (J = 1)$. From this we know that there is a phase transition at $J = 1$. We now compare our calculations of the NLCE with that of the exact result in 4.2.

To illustrate the method a bit more, we start by calculating the NLCE of order four (NLCE(O4)) by hand. At the moment we mean by NLCE of order four, that the biggest cluster we include has four vertices. Later we introduce another definition of the order, which can be motivated from perturbation theory. As explained in section two we start the NLCE by recursivly calculating the reduced energies starting with the smallest cluster.

For the chain the smallest cluster $G_1$ is just one vertex without any edges. However, the ground state energy of that cluster $E(G_1)$ is zero, because of the constant term we added in our hamiltonian.



Figure 4.1: A one dimensional lattice i.e. a chain: In one dimension there is only one type of lattice, where every vertex is connected to two neighbouring vertices. So the lattice looks like a chain. The dots in front and at the end indicate that this chain is of infinite length.

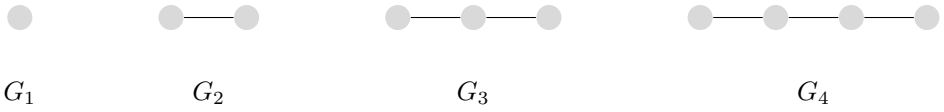


Figure 4.2: Subgraphs of a chain: The subgraphs of a one dimensional lattice are just chain segments of a certain length. Here the first 4 are shown. Where the smallest subgraph is just a vertex without any edges.

Therefore the reduced energy $\epsilon(G_1)$ is also zero. The next bigger graph is $G_2$ with two vertices and one edge between them. The reduced energy for this cluster is then

$$\epsilon(G_2) = E(G_2) - C(G_1)\epsilon(G_1) = E(G_2)$$

where we used, that $\epsilon(G_1) = 0$ in the last equality. From now on, we just leave out the contribution from $G_1$ because it is zero anyway. With that

$$\epsilon(G_3) = E(G_3) - C\left(\frac{G_2}{G_3}\right)\epsilon(G_2)$$

and

$$\epsilon(G_4) = E(G_4) - C\left(\frac{G_3}{G_4}\right)\epsilon(G_3) - C\left(\frac{G_2}{G_4}\right)\epsilon(G_2).$$

We can calculate the embedding factors with 4.1. Therefore,

$$C\left(\frac{G_2}{G_3}\right) = 2,\ C\left(\frac{G_2}{G_4}\right) = 3 \text{ and } C\left(\frac{G_3}{G_4}\right) = 2.$$

With all these we can approximate ground state energy in the thermodynamic limit by an NLCE of order 4 ($E_0^{(4)}$):

$$E_0^{(4)}/4 = \sum_{i=1}^{4} C\left(\frac{G_i}{G_4}\right)\epsilon(G_i)$$

Going to higher order NLCE's is then a straight forward procedure. In figure 4.3 we compared the results of an NLCE of order 20 to the exact solution from the Pfeuty paper 4.2. We see that the maximum deviation is at $J = 1$ and is of the order of $10^{-4}$. What we can also observe is that the deviations tend to grow as one approaches $J = 1$. This behavior is to be expected, because we know that the phase transition is at $J = 1$ and from the study of phase transitions one knows that the correlation length gets bigger as one approaches the phase transition and even diverges at the phase transition. This means that if we approach the phase transition, processes of higher order become more and more important, and these are not included in our NLCE, because it is an expansion of finite clusters. All in all $E_0^{(20)}$ is still a good approximation to the exact ground state energy $E_0$. The plot that is shown here, is similar to figure 2 in a paper by Schmidt and Yang [29] where they compared the method of gCUT to the exact solution. Comparing these two plots, one sees that the results from the NLCE are roughly one order of magnitude closer to the exact solution. Now that we have seen that the NLCE is a good approximation for the TFIM on the chain, we move on the more complicated geometries, namly the TFIM on a triangular lattice.

### 4.1.2 TFIM on a triangular lattice

For the triangular lattice things are not as easy as for the chain. The generation of subgraphs is really not trivial and there exists no analytic solution. For the triangular lattice it is also important to differentiate between ferromagnetic and antiferromagnetic interactions. For the chain we did not need to do this. For big $J$ or in the low field limit, in ground state, for the chain, all spins will line up in the ferromagnet and anti align in the antiferromagnet, as shown in figure 4.5. There is no conflict.

On the triangular lattice we must distinguish between both cases. The Ising model with antiferromagnetic bonds on the triangular lattice is a frustrated system. In this system we have topological

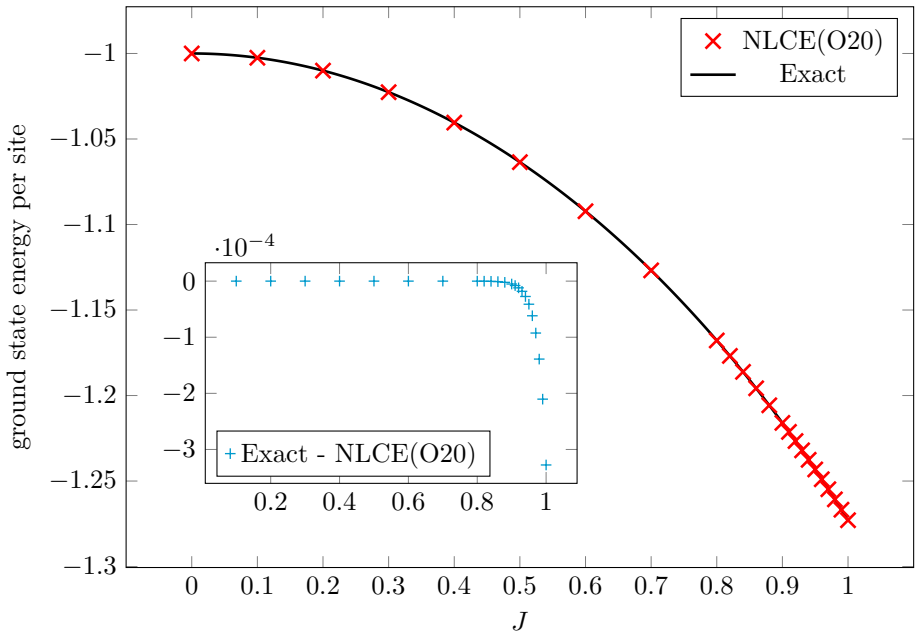


Figure 4.3: Ground state energy for the TFIM on a chain: The black line shows the exact result from Pfeuty 4.2. The red points were calculated from an NLCE of order 20. In the smaller plot we look at the deviation of the NLCE from the exact result, where we subtracted the NLCE datapoints from the exact points. In this plot one observes that the deviations grow as one approaches $J = 1$ and there the difference is largest with around $3 \cdot 10^{-4}$.


Figure 4.4: Ground state in the low field limit for the chain: For ferromagnetic interaction $J > 0$ all spins are aligned. For antiferromagnetic interactions $J < 0$ neighbouring spins will anti align.

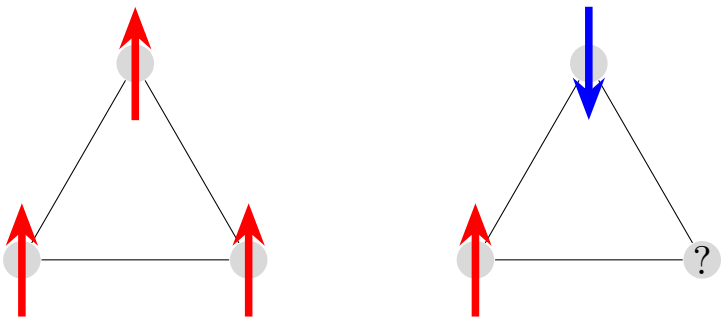


Figure 4.5: Ground state in the low field limit for a triangle: For ferromagnetic interaction $J > 0$ all spins are aligned. For antiferromagnetic interactions $J < 0$ neighbouring spins want to anti align. However, the spin at the bottom right corner, cannot mininize the bond energy with both of its neighbours. This spin is frustrated.

constraints, which "prevent neighbouring spins from adopting a configuration with every bond energy minimised" [30]. In figure 4.4 we see a simple subgraph of the triangular lattice with three vertices. For ferromagnetic interactions the ground state is either all spins pointing up or all down. However, for the antiferromagnet we cannot find a configuration, such that every bond energy is minimized. That this property, in the context of magnetic systems, has an important physical relevance was mentioned first by Gérard Toulouse in 1977 [31].

In addition, the number of subgraphs on the triangular lattice is growing exponentially. On the chain every spin has two neighbouring spins. A spin on the triangular lattice has six neighbouring spins. One says that the triangular lattice has a higher connectivity then the chain (the triangular lattice has the highest connectivity out of all Bravais lattices in two dimensions). For a chain of length 13 (13 vertices), one has 12 subgraphs, which are just the chain segments of length 12 or less. In contrast, there are 28765 connected subgraphs with 13 or less edges on the triangular lattice. Therefore, the NLCE on a triangular lattice is way more complex and computationally intense than for the chain.

However, from experience in perturbation theory one knows that not all graphs contribute equally. Some graphs have bigger contributions, others are negligible. For that reason, one often uses only a certain amount of graphs when doing graph based perturbative expansions. We denote these graphs as doubletouch graphs (DT graphs). It is an interesting question whether this also holds for the graph expansion in the NLCE. To check this, we compare an NLCE(O13,E13), with all graphs of order 13 or less, with maximally 13 edges, to an NLCE with DT graphs to order 13 (NLCE(O13,DT)) in perturbation theory. Before, we need to define this new ordering in perturbation theory. The order of a graph in perturbation theory is not determined by the number of vertices, but by the number of edges. However, there is one restriction. Every vertex needs to have an even degree. If there are vertices of odd degree one has to add edges, between vertices which are already connected by an edge, such that all vertices are of even degree. The least number of added edges together with the number of already existing edges defines the order of a graph in perturbation theory. Again to illustrate this new definition we look at a few basic examples. Figure 4.6 shows two graphs. The left graph $G$ has three vertices and three edges and is of order three in graph theory terms. To get the order in perturbation theory we need to look at the edges and degrees of the vertices. Every vertex is connected to two other vertices, thus each vertex is of degree two. So every vertex is of even degree and hence the graph is of order three in perturbation theory. For $G$ the two definitions of order coincide. Things change if we look at the right graph $G'$. $G'$ has three vertices and only two edges. Again in terms of graph theory the order is three. Looking at the degrees of the vertices we see that vertex $v_2'$ is even, but the vertices $v_1'$ and $v_3'$ are of odd degree. To make every vertex even, we need to add the two green edges. This is also the least number of additional edges one needs to add to achieve this. Therefore, graph $G'$ is of order four in perturbation theory. With that, we can now compare the results as stated before. In figure 4.7 we compare the results of an NLCE for the ferromagnetic TFIM on the triangular lattice. Once calculated with all graphs up to order 13, maximally 13 edges (NLCE(O13,E13)) and once calculated with all DT graphs up to order 13 in perturbation theory (NLCE(O13)(DT)). We see that the difference between both calculations is

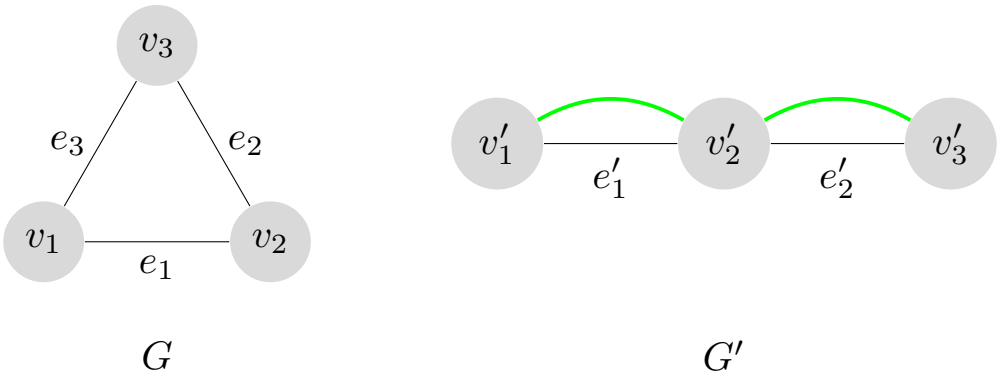


Figure 4.6: Order of graphs in perturbation theory: The left graph $G$ has 3 vertices, 3 edges and every vertex is of even degree. The order of graph is 3 and the order in perturbation theory is also 3. In the graph $G'$ these differ. $G'$ has 3 vertices and 2 edges. However, not all vertices are of even degree. While $v_2$ has an even degree, $v_1$ and $v_3$ are of the degree one. Therefore we need to add two additional edges, shown in green, to make every degree even. So graph $G'$ is of order 4 in perturbation theory.

of order $10^{-4}$. However, the calculation with all graphs is computationally way more expensive. For the NLCE(O13,E13) 28765 graphs need to be considered, whereas for the NLCE(O13,DT) we only need 1651. For that reason, most of the other calculations shown will be with DT graphs, because here we can go to higher orders and these higher order graphs are needed to get a good approximation if we are near the phase transition.

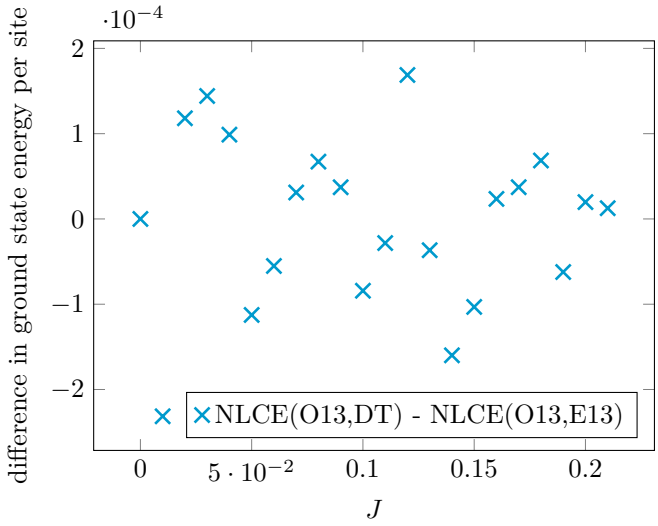


Figure 4.7: Comparison between Doubletouch graphs and all graphs: Here we calculated an NLCE for the ferromagnetic TFIM on the triangular lattice with all graphs up to order 13, with maximally 13 edges and an NLCE with all DT graphs up to order 13 in perturbation theory. The differences between those two are of order $10^{-4}$.

## Ferromagnetic TFIM

In figure 4.8 we compare the ground state energy calculations with an NLCE to a high temperature series expansion. The series was calculated by Matthias Mühlhauser to order 16 and we checked it with the series from the paper by Hamer and Oitmaa [32] up to order 14. Also from this paper we know that the phase transition for the ferromagnetic TFIM on the triangular lattice is at $J = 0.209$. Therefore, we calculated the NLCE for values up to $J = 0.21$. On the scale of $10^{-2}$ there is basically no difference between the NLCE(O16,DT) and the series of order 15 or 16. Looking at the small plot,

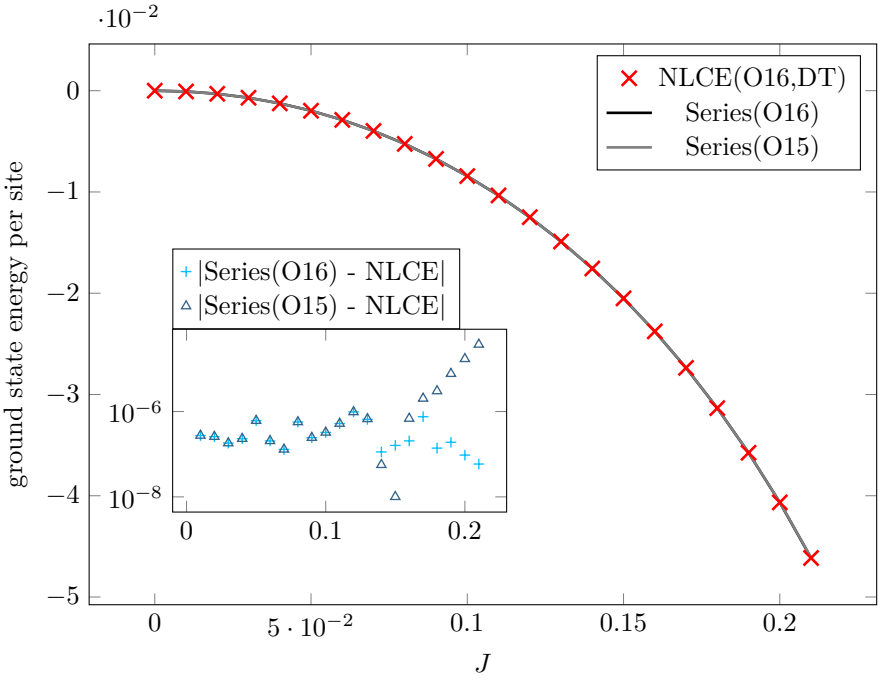


Figure 4.8: Ground state energy for the ferromagnetic TFIM on the triangular lattice: Here we compare the series expansion of order 15 and 16 to our NLCE with doubletouch graphs up to order 16. In the small plot the differences between both are shown. We see that the NLCE deviates more from the series expansions as we approach higher interaction strengths. For $J = 0.2$ the deviations are of order $10^{-4}$.

with a logarithmic y-axis, we see that the deviations from the series in order 16 and the NLCE are of the order of $10^{-6}$ for all $J$. However, if we compare the NLCE to the series of order 15, the deviations start to grow as one approaches the phase transition, which can again be explained by the increasing correlation length near the phase transition.

### Antiferromagnetic TFIM

For the antiferromagnetic TFIM we repeat the same steps for the ground state energy as we did for the ferromagnet. For the antiferromagnet the phase transition is around $J = 0.304$ [33][34]. In figure 4.9 we see that this time even at the scale of $10^{-2}$ the deviation is visible for values of $J$ near the phase transition. One also sees that the data points of the NLCE lie between the two series. In the small plot we again see the absolute differences between the series and the NLCE. Here one observes something interesting. For values below $J = 0.2$ the deviation of the NLCE to the series of order 16 is around $10^{-7}$, but then for $J > 0.2$ the deviations grow exponentially. The deviations to the series of order 15 start to grow a bit earlier and are one order of magnitude bigger.

Remember that the difference between the antiferromagnet and ferromagnet is the effect of frustration. However, not all subgraphs of the triangular lattices are affected by this. There exists a whole family of graphs for which frustration is not a concern, known as bipartite graphs. A graph is bipartite, if it does not have a cycle of odd order, where a cycle defines a path through the graph which starts and ends at the same vertex [35]. So for bipartite graphs, we can always find a configuration of spins such that every bond energy is minimized and thus they contribute in the same way for the antiferromagnet as for the ferromagnet. This could explain the behavior of the ground state energy for $J > 0.2$, because in a way these bipartite graphs may "sense" the phase transition of the ferromagnet.

## 4.1.3 Numerical Issues

In the previous sections we have seen that it is possible to calculate the ground state energy and that the results coincide with results gained with other techniques. It is still important to check the limitations and also the numerical stability of the method. To check the latter, we once again take into account the

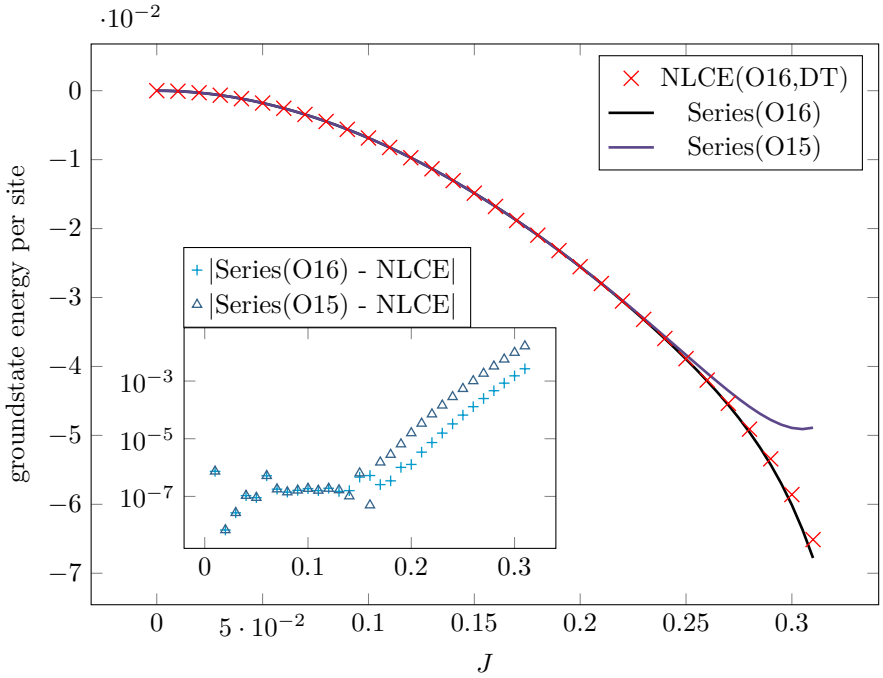


Figure 4.9: Ground state energy for the antiferromagnetic TFIM on the triangular lattice: Here we compare the series expansion of order 15 and 16 to our NLCE with doubletouch graphs up to order 16. In the small plot the differences between both are shown. Even on the scale of $10^{-2}$ the deviations of the NLCE to the series are visible. In the smaller plot we see a interesting behavior at around $J = 0.2$. Here the differences between the NLCE and the series start to grow exponentially.

calculations for the ferromagnetic TFIM on the triangular lattice. This time instead of plotting $J$ over the ground state energy per side, we look at a fixed $J$ and plot the additional contributions to the ground state energy per site $\Delta E_0^{(N)}$, for each order. These contributions are defined as $\Delta E_0^{(N)} = E_0^{(N)} - E_0^{(N-1)}$. So for example for the data point in figure 4.10 with the x-value $N = 3$ the y-value is the absolute difference between the NLCE(O3) and NLCE(O2). For the datapoints corresponding to $J = 0.05$ we see that the contributions at each order are decreasing exponentially up to order 12, but then abrubtly start to increase again. Whereas for $J = 0.15$ the contributions do not decrease as fast, because we are closer to the phase transition, but they do seem to behave in a smooth manner. It is important to note that the plot has a logarithmic y-axis. The fluctuations for the smaller $J$ start for a y-value in the order of $10^{-10}$ wheras the datapoints for $J = 0.15$ are five orders of magnitude higher for the same x-value. These fluctuations are caused by numerical instabilities. They arise due to a combination of a small error in the ED and the following multiplication by big embedding factors. The errors in the ED are of the order of $10^{-15}$ which is five orders of magnitude smaller then the scale where the fluctuations begin. However, for some subgraphs of the triangular lattice the embedding factor get extremly big. For the DT graphs up to order 16 on the triangular lattice the highest embedding factor is 1032153. Therefore, the error for the ground state energy of such a graph will be in the order of $10^{-9}$. If we take all graphs into considerations not just DT graphs, we have even higher embedding factors. The highest embedding factor for all graphs with 13 or less vertices is of the order of $10^7$. With that in mind, for small $J$, one should not include all contributions up to the highest order, but rather only use the values which are still numerically stable. It is nonetheless important to improve the numerical stability because near the phase transition the clusters of higher order become important. One idea would be to do all calculation not with double precision floating point numbers, and instead with a higher precision. However, at least for the algorithm we currently use, this is not scaleable.

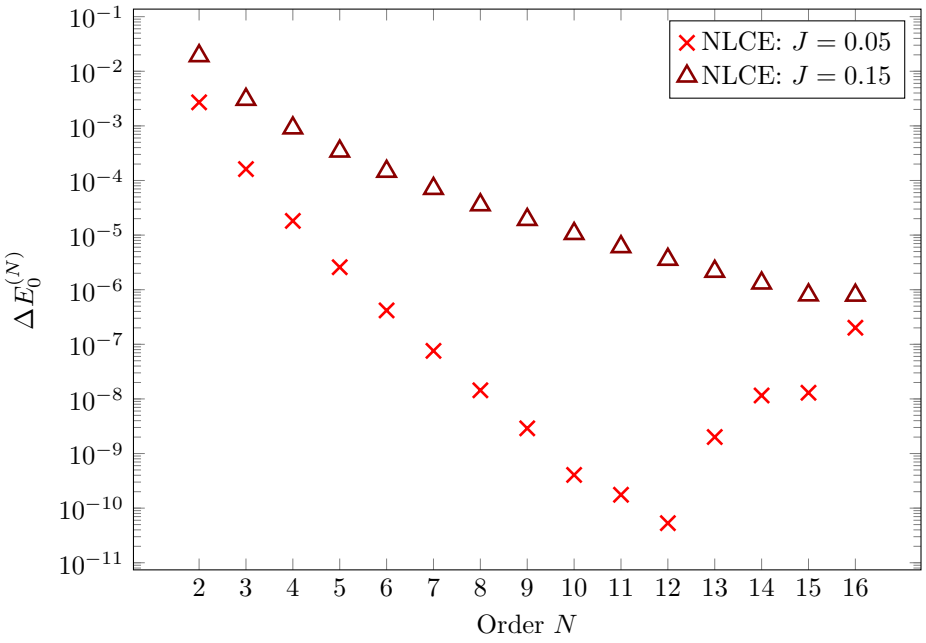


Figure 4.10: Additional contributions to the ground state energy $\Delta E_0^{(N)}$ ($\Delta E_0^{(N)} = E_0^{(N)} - E_0^{N-1}$) for the ferromagnetic TFIM at different orders $N$: For a small $J$, here $J = 0.05$ (red cross datapoints), the contributions decrease exponentially till order 12, but then start to grow again. This behavior is caused by numerical instabilities in the algorithm. For $J = 0.15$ (dark red and triangular datapoints) the contributions fall off continuously. Therefore for small $J$ it is better to cut off the NLCE at a certain order.

## 4.2 Second derivative ground state energy

The phase transition of the TFIM is of second order. From the discussion in chapter two we know that one expects that the second derivative of the ground state energy should not be continous at the phase transition. For the TFIM one knows that the second derivative diverges. For the chain this divergence grows only logarithmically, but for the triangular lattice it scales algebraically. This means that that $\frac{\mathrm{d}^2 E}{\mathrm{d}J^2} \propto (J - J_C)^{-\alpha}$ for $J$ near the the phase transition ($J_C$). In statitical mechanics the second derivative of the free energy with respect to temperature is usually called heat capicity ($C$). From this language we also name the second derivative of the ground state energy with respect to $J$ $C$. In this section we calculate the second derivative of the ground state energy, by means of finite differences (equation 4.3).

$$C = \frac{\mathrm{d}^2 E}{\mathrm{d}J^2}(J) = E(J - \Delta J) - 2E(J) + E(J + \Delta J) + O(\Delta J^2) \tag{4.3}$$

For most calculations we have chosen a discretization $\Delta J = 0.01$. We also try to extract the critical exponent $\alpha$.

### Ferromagnetic TFIM

In figure 4.11 we see the results of the finite differences calculation for the second derivative of the ground state energy. Again we compare these to the second derivative of the series expansions. The differences between these are a couple of orders magnitude bigger than for the ground state energy and we see again the trend that the deviations from the series of order 15 grow as we approach the phase transition. However, both the series and the NLCE are perfectly continuous around the value of the phase transition, which is perfectly reasonable because we look at finite systems and the statement from chapter two about the non-analycity in the ground state energy is only true in the thermodynamic limit, i.e. on an infinite system. Nonetheless, we still want to try to calculate the critical exponent. To achieve this we do a similar plot as we have done in the numerical issues section. We look at the additional contributions to the second derivative, at the phase transition, at different orders. The additional contributions we label

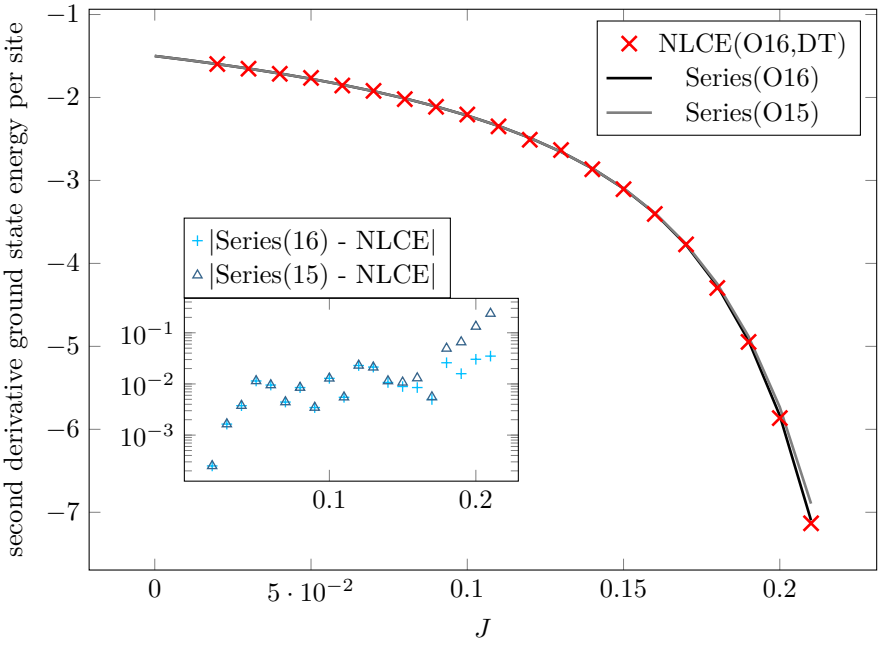


Figure 4.11: Second derivative of the ground state ($C$) per site for the ferromagnetic TFIM: Here we compare the second derivative of the series and the second derivative of the NLCE, calculated with finite differences with a discretization $\Delta J = 0.01$. The deviations from those are orders of magnitude bigger than for the ground state energy and one sees the same trend that the deviations grow with the order 15 series grows as one approaches the phase transition.

as $\Delta C^{(N)} = C^{(N)} - C^{(N-1)}$. Then we try to fit an algebraic function $f(J) \propto J^{-\kappa}$ to the data points. From the theory of generalized homogeneous functions [36], we expect that the exponent $\kappa$ from our fit is related to $\alpha$ via

$$\kappa = 1 - \frac{\alpha}{\nu} \tag{4.4}$$

if the order of our graphs scales as a length. The exponent $\nu$ is the critical exponent of the correlation length. In figure 4.12 we fitted such an algebraic function to the values of $N$ between 10 and 15 and get $\kappa = 0.87$ as an exponent. Plugging this into equation 4.4 we get a value for $\frac{\alpha}{\nu} = 0.13$. The literature value for $\frac{\alpha}{\nu}$ is 0.157 [32]. From that we see that we can use the NLCE and extract the right scaling behavior atleast within a factor of two. We also tried to vary the values used for the fit and also the discretization. In Appendix B we summarized all the many different combinations of chosen data points and discretization. In general for $\Delta J = 0.01$ or $\Delta J = 0.05$ the fitting method is stable and we get an exponent of roughly 0.9. For smaller discretizations ($\Delta J = 0.001$) we see bigger fluctuations. The exponent also varies slightly if one changes the number of data points used for the calculation of the fit, but because we want to look at a scaling at the phase transition we have chosen to only include higher order data points in our fit. We excluded the order 16 data points, because this data point seems to be numerically unstable.

## Antiferromagnetic TFIM

We now repeat the process for the antiferromagnetic TFIM. In figure 4.13 one immediately observes that for the antiferromagnet the deviations are much bigger than for the ferromagnet. In the small plot we also see that deviations start growing from the start even for small $J$. If we look at the additional contributions to the second derivative at different orders, as shown in figure 4.14, we see that those have an alternating sign. For even $N$ the contributions are negative, while for odd $N$ the contributions are positive. We can also observe for $J = 0.15$ the contributions fall off for high orders and eventually go to zero. However, for $J = 0.22$, which is still far away from the phase transition of the antiferromagnet(at $J = 0.304$), but close to the phase transition of the ferromagnet, the contributions do not fall off and even start to grow again. This behavior is probably linked to the deviations in the ground state energy

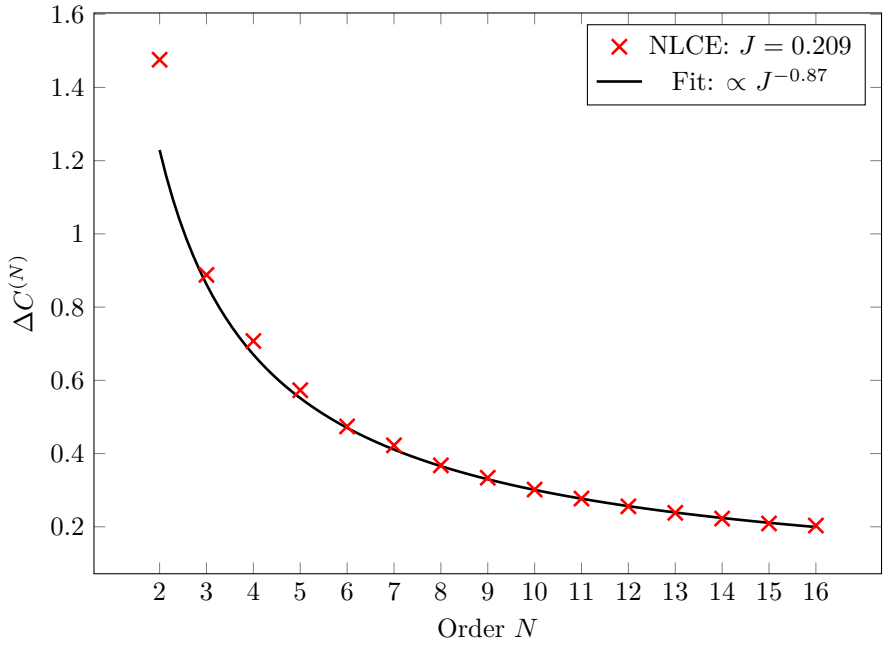


Figure 4.12: Additional contributions to the second derivative of the ground state energy $C^{(N)}$ for the ferromagnetic TFIM at different orders $N$: These contributions fall off as we go to higher and higher orders. As expected for $J = 0.209$, at the phase transitions, the contributions decrease algebraically $\propto J^{-\kappa}$. From the fitted curve we see that exponent $\kappa = 0.87$.

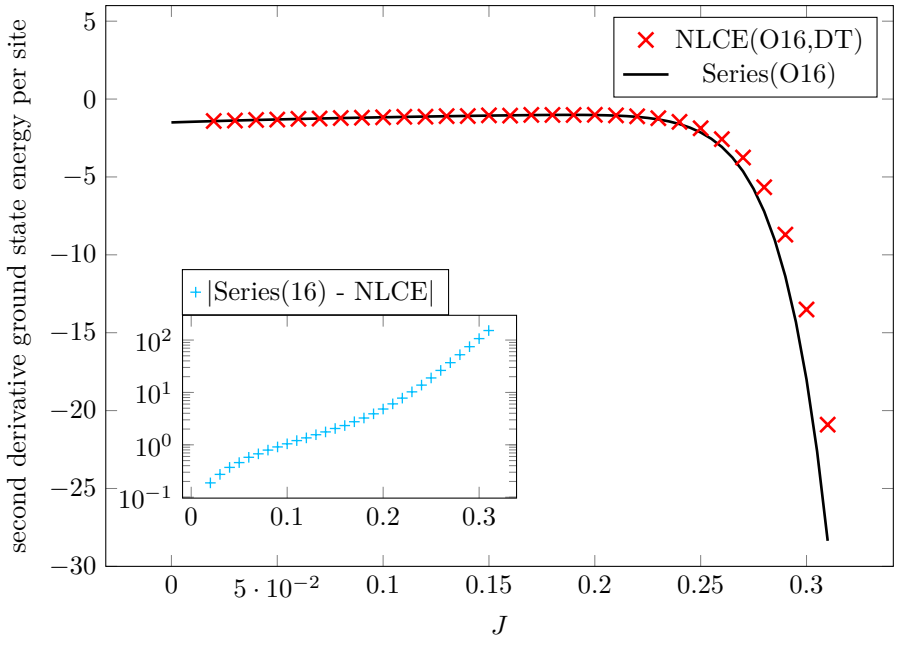


Figure 4.13: Second derivative of the groundstate energy ($C$) per site for the antiferromagnetic TFIM: Here we compare the second derivative of the series and the second derivative of the NLCE, calculated with finite differences. The deviations of the series and the NLCE are way bigger than for the ferromagnet and these deviations are growing with increasing $J$.

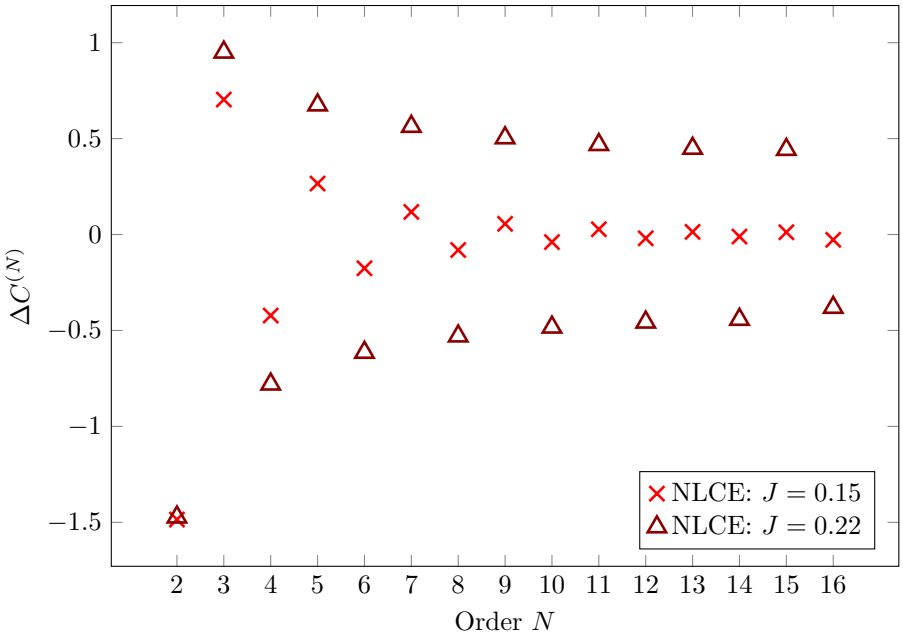


Figure 4.14: Additional contributions to the second derivative of the ground state energy $C^{(N)}$ for the antiferromagnetic TFIM at different orders $N$: The contributions have an alternating sign for different $N$. For even $N$ the additional contributions are negative and for odd $N$ the contributions are positive. For $J = 0.15$ the additional contributions are falling as $N$ gets bigger and eventually drop nearly to zero. However, for J=0.22 still far away from the phase transition the contributions do not fall off and instead start to growing again around $N = 10$.

which also started for a $J$ around 0.21. Thus, we cannot calculate critical exponents as we did for the ferromagnetic TFIM.

# Chapter 5

# Conclusions and Outlook

In this thesis we investigated the method of numerical linked cluster expansions. We showed that this method is a powerful tool for calculating the ground state energy for the transverse field Ising model and that the results coincide with calculations done with other methods. It was also interesting to see that the DT graph expansion motivated from perturbation theory, gave also good results for the NLCE. Additionally we saw that in principal it is also possible to extract critical exponents and that the expansion scales in the right way. However, we found out that there can be limitations or restrictions. While we have obtained good results in the calculations for the ferromagnetic TFIM on the triangular lattice, the calculations for the antiferromagnet showed that it might not be as easy to set up the graph expansion for frustrated systems, where different families of graphs can behave in different ways. In the future it might be interesting to understand this behavior in more detail. One could set up a graph expansion for the triangular lattice not with all graphs or DT graphs, but rather select specific graphs which might be better suited for the frustrated system. One idea would be to try to leave out the bipartite graphs and see how the results for the NLCE change. Such an expansion also reduces the number of subgraphs drastically which would be save computation time. Thus one might be able include relevant graphs of higher order. Computationally it would also be interesting to see whether one can improve the numerical stability. Overall numerical linked cluster expansions seem to be a good alternative to other techniques and it will be an interesting to see if one finds better graph expansions such that we also get the right scaling behavior for frustrated systems like the antiferromagnetic TFIM on the triangular lattice.

# Appendix A

# Julia Programming Language

The Julia Programming language is a relativly new programming language. It was introduced in 2012 as an open source project by Jeff Bezanson, Stefan Karpinski, Viral B. Shah and Alan Edelman. Julia is an attempt to solve the two language problem. In physics and also engineering or data science many programmers prefer high-level dynamic languages like MATLAB, R or Python. In these languages code is easy to write and read, but one has the drawback of losing performance compared to compiled languages like C or Fortran. Julia is a JIT compiled language (just in time) which tries to bridge this gap between easy to write and read and still being performent. More information can be found in [37]. In this thesis all the code was written in Julia and can be found on GitHub [38].

# Appendix B

# Algebraic fit

In chapter four we looked at the scaling behavior for the ferromagnetic TFIM and fitted an algebraic function $f(J) \propto J^{-\kappa}$ to the datapoints. From this we calculated $\frac{\alpha}{\nu}$. For the plot in this chapter we used the data points from $N = 10$ till $N = 15$ and a discretization of $\Delta J = 0.01$. However, we also tried out different combinations of data points and discretizations to look at the stability of the method. In table B.1 we have listed all combinations we tried. The row number M indicates the first datapoint chosen and the column number N the last datapoint. In every row are three values for the exponent $\kappa$. For the first value the discretization is $\Delta J = 0.001$. For the second $\Delta J = 0.005$ and for the last $\Delta J = 0.01$. We only included exponents in this table when we had atleast 3 datapoints to fit, therefore some of the entries in the table are empty.

| | N = 8 | N = 9 | N = 10 | N = 11 | N = 12 | N = 13 | N = 14 | N = 15 | N = 16 |
|---|---|---|---|---|---|---|---|---|---|
| | 1.02 | 1.01 | 1.01 | 1.0 | 0.99 | 0.99 | 0.98 | 0.9 | 0.67 |
| M = 2 | 1.02 | 1.01 | 1.01 | 1.0 | 1.0 | 1.0 | 0.99 | 0.99 | 0.98 |
| | 1.02 | 1.01 | 1.0 | 1.0 | 1.0 | 0.99 | 0.99 | 0.99 | 0.98 |
| | 0.9 | 0.9 | 0.9 | 0.9 | 0.9 | 0.89 | 0.88 | 0.74 | 0.3 |
| M = 3 | 0.9 | 0.9 | 0.9 | 0.91 | 0.91 | 0.91 | 0.91 | 0.91 | 0.89 |
| | 0.89 | 0.9 | 0.9 | 0.9 | 0.9 | 0.9 | 0.9 | 0.9 | 0.89 |
| | 0.94 | 0.94 | 0.94 | 0.93 | 0.92 | 0.91 | 0.88 | 0.66 | -0.09 |
| M = 4 | 0.94 | 0.94 | 0.94 | 0.94 | 0.94 | 0.94 | 0.93 | 0.93 | 0.89 |
| | 0.93 | 0.93 | 0.93 | 0.93 | 0.93 | 0.92 | 0.92 | 0.92 | 0.91 |
| | 0.93 | 0.93 | 0.93 | 0.92 | 0.9 | 0.89 | 0.85 | 0.5 | -0.76 |
| M = 5 | 0.93 | 0.93 | 0.93 | 0.93 | 0.93 | 0.93 | 0.93 | 0.93 | 0.87 |
| | 0.92 | 0.92 | 0.92 | 0.92 | 0.91 | 0.91 | 0.91 | 0.91 | 0.89 |
| | | 0.9 | 0.9 | 0.9 | 0.87 | 0.86 | 0.8 | 0.3 | -9.77 |
| M = 6 | | 0.9 | 0.9 | 0.91 | 0.91 | 0.92 | 0.91 | 0.92 | 0.83 |
| | | 0.89 | 0.89 | 0.89 | 0.9 | 0.9 | 0.9 | 0.89 | 0.87 |
| | | | 0.95 | 0.92 | 0.87 | 0.86 | 0.77 | 0.04 | -9.78 |
| M = 7 | | | 0.94 | 0.94 | 0.94 | 0.94 | 0.93 | 0.94 | 0.94 |
| | | | 0.93 | 0.93 | 0.92 | 0.92 | 0.92 | 0.91 | 0.87 |
| | | | | 0.69 | 0.81 | 0.8 | 0.69 | 0.35 | -9.82 |
| M = 8 | | | | 0.92 | 0.92 | 0.93 | 0.92 | 0.92 | 0.75 |
| | | | | 0.9 | 0.9 | 0.9 | 0.9 | 0.89 | 0.84 |
| | | | | | 0.76 | 0.77 | 0.61 | -0.87 | -9.92 |
| M = 9 | | | | | 0.94 | 0.95 | 0.93 | 0.94 | 0.69 |
| | | | | | 0.92 | 0.92 | 0.92 | 0.89 | 0.82 |
| | | | | | | 0.69 | 0.48 | -1.62 | -10.12 |
| M = 10 | | | | | | 0.94 | 0.91 | 0.93 | 0.59 |
| | | | | | | 0.91 | 0.91 | 0.87 | 0.78 |
| | | | | | | | 0.32 | -2.66 | -10.47 |
| M = 11 | | | | | | | 0.91 | 0.93 | 0.43 |
| | | | | | | | 0.91 | 0.86 | 0.73 |
| | | | | | | | | -4.12 | -10.99 |
| M = 12 | | | | | | | | 0.93 | 0.19 |
| | | | | | | | | 0.83 | 0.64 |

Table B.1: Different combinations of data points and discretizations

# Danksagung

Ich würde mich noch gerne bei einigen Leuten bedanken. Zum einem bei Kai Schmidt, für die Auswahl meines Thema und für die enge Betreuung während den drei Monaten. Die Diskussionen waren immer hilfreich und lehrreich. Großer Dank geht auch an Matthias Mühlhauser für die Generation aller Graphen und auch für die Hilfe bei jeglichen Fragen diesbezüglich und auch anderer Themen. Auch will ich mich noch bei Jan und Max bedanken, die bei einigen Diskussionen immer gute Ratschläge hatten. Zuletzt noch großer Dank an Janika, für die tolle Unterstützung während den drei Monaten.

# Bibliography


[1] A. Einstein, *Über die allgemeine Relativitätstheorie*. Springer, 2009.

[2] P. W. Anderson, "More is different," *Science*, vol. 177, pp. 393–396, 1972.

[3] J. Oitmaa, C. Hamer, and W. Zheng, *Series expansion methods for strongly interacting lattice models*. Cambridge University Press, 2006.

[4] A. W. Sandvik and J. Kurkijärvi, "Quantum monte carlo simulation method for spin systems," *Physical Review B*, vol. 43, no. 7, p. 5950, 1991.

[5] M. Rigol, T. Bryant, and R. R. Singh, "Numerical linked-cluster approach to quantum lattice models," *Physical review letters*, vol. 97, no. 18, p. 187202, 2006.

[6] K. Coester, S. Clever, F. Herbst, S. Capponi, and K. Schmidt, "A generalized perspective on non-perturbative linked-cluster expansions," *EPL (Europhysics Letters)*, vol. 110, no. 2, p. 20006, 2015.

[7] S. J. Blundell, *Magnetism: a very short introduction*. OUP Oxford, 2012.

[8] D. C. Mattis, "History of magnetism," in *The Theory of Magnetism I*, pp. 1–38, Springer, 1981.

[9] W. Gilbert, *De magnete*. Courier Corporation, 1958.

[10] J. C. Maxwell, *A treatise on electricity and magnetism*, vol. 1. Clarendon press, 1873.

[11] S. G. Brush, "History of the lenz-ising model," *Reviews of modern physics*, vol. 39, no. 4, p. 883, 1967.

[12] L. Onsager, "Crystal statistics. i. a two-dimensional model with an order-disorder transition," *Physical Review*, vol. 65, no. 3-4, p. 117, 1944.

[13] G. Jaeger, "The ehrenfest classification of phase transitions: introduction and evolution," *Archive for history of exact sciences*, vol. 53, no. 1, pp. 51–81, 1998.

[14] P. De Gennes, "Collective motions of hydrogen bonds," *Solid State Communications*, vol. 1, no. 6, pp. 132–137, 1963.

[15] R. B. Stinchcombe, "Ising model in a transverse field. i. basic theory," *Journal of Physics C: Solid State Physics*, vol. 6, pp. 2459–2483, 8 1973.

[16] D. Chandler, "Introduction to modern statistical," *Mechanics. Oxford University Press, Oxford, UK*, vol. 5, p. 449, 1987.

[17] N. Deo, *Graph theory with applications to engineering and computer science*. Courier Dover Publications, 2017.

[18] J. E. Mayer and E. Montroll, "Molecular distribution," *The Journal of Chemical Physics*, vol. 9, no. 1, pp. 2–16, 1941.

[19] B. H. Zimm, "Joseph edward mayer," 1994.

[20] R. P. Feynman, "Space-time approach to quantum electrodynamics," in *Quantum Electrodynamics*, pp. 178–198, CRC Press, 2018.

[21] L. Marland, "Series expansions for the zero-temperature transverse ising model," *Journal of Physics A: Mathematical and General*, vol. 14, no. 8, p. 2047, 1981.

[22] A. Irving and C. Hamer, "Abelian lattice gauge theories in 3+ 1 dimensions: The linked cluster approach," *Nuclear Physics B*, vol. 240, no. 3, pp. 362–376, 1984.

[23] C. Knetter, K. P. Schmidt, and G. S. Uhrig, "The structure of operators in effective particle-conserving models," *Journal of Physics A: Mathematical and General*, vol. 36, no. 29, p. 7889, 2003.

[24] K. Coester and K. Schmidt, "Optimizing linked-cluster expansions by white graphs," *Physical Review E*, vol. 92, no. 2, p. 022118, 2015.

[25] B. Tang, E. Khatami, and M. Rigol, "A short introduction to numerical linked-cluster expansions," *Computer Physics Communications*, vol. 184, no. 3, pp. 557–564, 2013.

[26] Y. Saad, *Iterative methods for sparse linear systems*. SIAM, 2003.

[27] B. Zeng, X. Chen, D.-L. Zhou, X.-G. Wen, *et al.*, *Quantum information meets quantum matter*. Springer, 2019.

[28] P. Pfeuty, "The one-dimensional ising model with a transverse field," *ANNALS of Physics*, vol. 57, no. 1, pp. 79–90, 1970.

[29] H.-Y. Yang and K. P. Schmidt, "Effective models for gapped phases of strongly correlated quantum lattice models," *EPL (Europhysics Letters)*, vol. 94, no. 1, p. 17004, 2011.

[30] J. Vannimenus and G. Toulouse, "Theory of the frustration effect. ii. ising spins on a square lattice," *Journal of Physics C: Solid State Physics*, vol. 10, no. 18, p. L537, 1977.

[31] G. Toulouse *et al.*, "Theory of the frustration effect in spin glasses: I," *Spin Glass Theory and Beyond: An Introduction to the Replica Method and Its Applications*, vol. 9, p. 99, 1987.

[32] H.-X. He, C. Hamer, and J. Oitmaa, "High-temperature series expansions for the (2+ 1)-dimensional ising model," *Journal of Physics A: Mathematical and General*, vol. 23, no. 10, p. 1775, 1990.

[33] M. Powalski, "Quantum paramagnetism in the kagome and triangular transverse field ising model," 2012.

[34] M. Powalski, K. Coester, R. Moessner, and K. Schmidt, "Disorder by disorder and flat bands in the kagome transverse field ising model," *Physical Review B*, vol. 87, no. 5, p. 054404, 2013.

[35] A. S. Asratian, T. M. Denley, and R. Häggkvist, *Bipartite graphs and their applications*, vol. 131. Cambridge university press, 1998.

[36] A. Hankey and H. E. Stanley, "An alternate formulation of the static scaling hypothesis," 1971.

[37] J. Bezanson, S. Karpinski, V. B. Shah, and A. Edelman, "Julia: A fast dynamic language for technical computing," *arXiv preprint arXiv:1209.5145*, 2012.

[38] "https://github.com/mpirke/nlce.jl."

# Declaration

I declare that I have written the thesis by myself and that no sources or aids other than those quoted in this thesis have been used.

*Erlangen, 05.August.2022*

Markus Pirke